

A multi-proxy inference of Jōmon population dynamics using Bayesian phase models, residential data, and summed probability distribution of ^{14}C dates

Enrico R. Crema (University of Cambridge)
Ken'ichi Kobayashi (Chūō University)

Abstract

We introduce a new workflow for analysing archaeological frequency data associated with relative rather than absolute chronological time-stamps. Our approach takes into account multiple sources of uncertainty by combining Bayesian chronological models and Monte-Carlo simulation to sample possible calendar dates for each archaeological entity. We argue that when applied to settlement data, this combination of methods can bring new life to demographic proxies that are currently under-used due to their lack of chronological accuracy and precision, and provide grounds for further exploring the limits and the potential of the so-called “dates as data” approach based on the temporal frequency of radiocarbon dates. Here we employ this new workflow by re-examining a legacy dataset that has been used to describe a major population rise-and-fall that occurred in central Japan during the Jōmon period (16,000 - 2,800 cal BP), focusing on the temporal window between 8,000 and 3,000 cal BP. To achieve this goal we: 1) construct the first Bayesian model of forty-two Jōmon ceramic typology based cultural phases using a sample of 2,120 radiocarbon dates; 2) apply the proposed workflow on a dataset of 9,612 Jōmon pit-dwellings; and 3) compare the output to a Summed Probability Distribution (SPD) of 1,550 radiocarbon dates from the same region. Our results provide new estimates on the timing of major demographic fluctuations during the Jōmon period and reveal a generally good correlation between the two proxies, although with some notable discrepancies potentially related to changes in settlement pattern.

Key Highlights

- A new approach for characterising temporal frequency of archaeological data is proposed.
- The first Bayesian chronological model of Jōmon phases is presented.
- The fluctuations in the number of Jōmon pit-dwellings in the western Kanto region is re-examined.
- Demographic inference based on counts of pit-dwellings is compared to summed probability distribution of radiocarbon dates.

Keywords

Bayesian Chronological Modelling; Monte-Carlo Simulation; Jōmon Chronology; Prehistoric Demography

39 Introduction

40 The last decade witnessed an increasing number of synthetic research studies (Kintigh et al.
41 2014) where legacy archaeological data, originally collected for different purposes, have been
42 brought together for new purposes. Given the finite nature of the archaeological record
43 (Surovell et al. 2017), it is our collective responsibility to identify opportunities for data reuse,
44 as well as tackle the new types of methodological and theoretical hurdles prompted by this
45 task (Bevan 2015, Huggett 2020). Perhaps one of the best examples of such new challenges
46 is the reuse of large collections of radiocarbon dates as a proxy of prehistoric demographic
47 changes. This approach, often referred to as *dates as data* (Rick 1987), has grown rapidly in
48 its number of applications during the last decade (e.g. Shennan et al. 2013, Crema et al. 2016,
49 Zahid et al. 2016, Bevan et al. 2017, Riris 2018 etc.), thanks to the increased availability and
50 accessibility of radiocarbon databases (e.g. Chaput and Gajewski 2016, Manning et al. 2016,
51 Lucarini et al. 2020) and the parallel development of a suite of new statistical techniques
52 designed to handle such data (Brown 2017, Crema et al. 2016, Crema et al. 2017, Bronk
53 Ramsay 2017, Timpson et al. 2014, McLaughlin 2018, etc.).

54

55 The *dates as data* approach is, however, not immune to criticisms. Its core assumption (more
56 people → more dateable samples → more radiocarbon dates) has been critically discussed
57 since its inception (see fig.1 in Rick 1987), and several issues have been put forward in the
58 last decade, from the false signals linked to sampling error and the calibration process to
59 deeper concerns on the very nature of the proxy itself (e.g. Attenbrow and Hiscock 2015,
60 Contreras and Meadows 2014, Freeman et al. 2018, Torfing 2015, Williams 2012, Weninger
61 et al. 2015). While methodological advances have solved many of these challenges, some
62 remain sceptical of the usefulness of the whole enterprise. There is, however, a consensus
63 amongst practitioners (and critics), that prehistoric population reconstructions should be based
64 on multiple proxies rather than be exclusively reliant on the density of radiocarbon dates.
65 Nonetheless, examples are limited (but see Crombé and Robinson 2014, Downey et al. 2014,
66 Palmisano et al. 2017, Tallavaara and Pesonen 2018, Feeser et al. 2019), as most alternative
67 proxies in prehistoric contexts do not offer comparable chronological precision and accuracy
68 to radiocarbon dates. As a consequence, more traditional and perhaps more direct lines of
69 evidence such as site and dwelling counts have been underused due to their temporal
70 definition being based on attributions to cultural phases rather than absolute dates (but see
71 Oh et al. 2017).

72

73 *Uncertainties in Archaeological Periodisations*

74 In order to be able to use proxies that are exclusively defined by chrono-typological phases,
75 we need to be able to assign to each calendar date t a probability of occurrence $P(t)$ of an
76 archaeological event. The objective is thus fundamentally equivalent to the calibration of

77 radiocarbon dates; both measure some physical properties (amount of ^{14}C isotope vs
78 diagnostic traits on artefacts) linked to the flow of time through some process (radiocarbon
79 decay vs cultural transmission) and make use of a statistical model that combines different
80 sources of uncertainty to yield a probabilistic estimate of when a particularly event has
81 occurred (e.g. making a ceramic vessel). In the case of radiocarbon calibration, these are
82 measurement errors in the sample and the uncertainties associated with the calibration curve.
83 In the case of archaeological periodisation, we need to take into account three interrelated
84 forms of uncertainty.

85

86 The first one, which we will refer here to as *within-phase uncertainty*, is how we define the
87 shape of the probability density function within the archaeological period assigned to a
88 particular event. In other words, how we describe the change of $P(t)$ when t is within a
89 particular phase? For example, if an event is assigned to a phase dated between 700 and 300
90 BC, what is the probability that the event occurred in the year 354 BC? While ultimately the
91 selection of the most appropriate probability density function is context-dependent, there have
92 been some discussions on what shape we should assume a priori. Proponents of aoristic
93 analysis (e.g. Johnson 2004, Crema 2012, Orton et al. 2017) suggest a uniform distribution,
94 and hence would assign a constant probability within the archaeological phase (thus for the
95 example above, $P(t=354 \text{ BC})$ would be equal to 0.0025, or $1/400$). Crema (2012) justifies this
96 shape invoking the principle of insufficient reason: in the lack of any additional knowledge, we
97 should assume that all years have equal probabilities. This assumption may be valid in crime
98 science (where the aoristic analysis was originally developed, see Ratcliffe and McCullagh
99 1998), and perhaps in some historical contexts where an ensemble of chrono-typological,
100 dendrochronological, numismatic, and historical dates are available. However, for prehistoric
101 chrono-typological phases, there is a reasonably large number of theoretical and empirical
102 studies (e.g. Rogers 1962, Christenson 1994, Neiman 1995, Lyman and Harpole 2002,
103 Manning et al. 2015, Kandler and Crema 2019, etc.) that suggest a unimodal curve of a rise
104 and fall in popularity (referred to as popularity principle; see O'Brien and Lyman 2000) to be
105 more appropriate. The literature on chronological apportioning, which deals with similar
106 problems, has indeed adopted such assumption by using probability distributions such as the
107 Chi-square (Carlson 1983), the Gamma (Steponaitis and Kintigh 1993), the Beta (Baxter and
108 Cool 2016), and the normal distributions (both in its truncated or non-truncated forms; Carlson
109 1983, Bellanger and Husi 2012, Roberts et al. 2012, Baxter and Cool 2016). These
110 alternatives reflect both the general agreement on the unimodal shape and the more context-
111 specific debate on whether the rise and fall in popularity should be assumed to be symmetric
112 or not, or whether there should be flexibility in capturing variation in the kurtosis.

113

114 The second form of uncertainty is determined by how we define the membership of a particular
115 archaeological event to a given archaeological phase or period. This type of uncertainty (see
116 Bevan et al. 2012, Crema 2015 for review), which we will refer here to as *phase assignment*
117 *uncertainty*, is conditioned by the nature of the diagnostic elements used by archaeologists to
118 associate a particular artefact to an archaeological phase. An event can thus be assigned to
119 one or more phases or subphases, with potentially high levels of non-random inter-observer
120 errors (see Bevan et al. 2012 for an example involving potsherd recovered in survey contexts).
121 *Phase assignment uncertainty* is effectively linked with *within-phase uncertainty*, as one could
122 argue that $P(t)$ could be described by a mixture model with k probability density functions,
123 each with a mixture weight which are probabilities that sum to unity. The parameter k will thus
124 represent the range of possible chrono-typological phases, and the weights would represent

125 our degree of belief of a focal event being assigned to each. Estimates of the mixture weights
126 could potentially be derived from properties of the diagnostic elements (see for example Bevan
127 et al. 2012), but in the majority of cases these are unlikely to be reported (i.e. most
128 archaeologists will report “phase A ~ phase B”, rather than “70% phase A and 30% phase B”).
129 It is an open question on whether in the absence of precise mixture weights one should
130 assume them to be uniformly distributed, proportional to the duration of each phase (e.g. if
131 phase B has three times the duration of phase A, w_A should be equal to 0.25 and w_B equal to
132 0.75), or based on observed frequencies of artefacts assigned to each phase (cf Ortman
133 2014).

134

135 The third form of uncertainty is determined by how the phases themselves are dated. Can we
136 be confident that the phase to which we assigned our event is precisely dated between 700
137 and 300 BC, rather than 711 and 298 BC? In essence, such *phase boundary uncertainty* is
138 associated with our uncertainty in defining the parameters of the probability density function
139 describing each phase. Nearly three decades of Bayesian chronological models of
140 radiocarbon dates (Buck et al. 1992, Ziedler et al. 1998, Bronk Ramsey 2009a) have dealt
141 with this problem, enabling archaeologists to infer parameters for a variety of distributions
142 (including flexible options such as the trapezoidal distribution, Lee and Bronk Ramsey 2012),
143 as well as to incorporate various assumptions in the form of priors and constraints.

144

145 Thus, there is a substantial body of archaeological work that tackles these three forms of
146 uncertainties, but little to no attempt has been made to take them into account at the same
147 time. We argue that such partial treatment can lead to substantial biases when examining
148 frequency data. For example, handling *within-phase uncertainty* but ignoring *phase boundary*
149 *uncertainty* might potentially lead to the false impression that significant changes in temporal
150 frequencies occur at precise intervals corresponding to boundaries between archaeological
151 phases¹.

152

153 The solution proposed in this paper expands the Monte-Carlo approach developed initially in
154 Crema 2012 by utilising Bayesian posterior samples of phase parameters. This effectively
155 involves simulating n possible dates of archaeological events by iteratively: 1) sampling a
156 random start and end date of the assigned phase(s) (*phase boundary uncertainty*); 2)
157 randomly assign the event to a unique phase (*phase assignment uncertainty*); and 3) randomly
158 sample a possible date within such phase (*within-phase uncertainty*). In order to enable full
159 reproducibility (Marwick 2017), details of this procedure, as well as the R and OxCal scripts
160 utilised for the case study, are available on the following GitHub repository:
161 <https://github.com/ercrema/jomonPhasesAndPopulation> as well as on zenodo:
162 <https://doi.org/10.5281/zenodo.3719507>

163 *Case Study: Jōmon Chronology and Demography*

164 The Jōmon culture (16,000 - 2,800 cal BP) offers one of the best researched prehistoric
165 hunter-gatherer traditions known to archaeology, thanks to the exceptionally high volume of
166 rescue archaeology in Japan (Habu and Okamura 2017) combined with the rare opportunity

¹ It is also worth noting here that while the formal definitions of these different forms of chronological uncertainties are pivotal in designing the solution detailed below, we are not implying here an essentialist approach towards typological phases, but rather acknowledge them as useful abstractions that capture observed continuous variations of diagnostic elements and their relation to the flow of time.

167 to rely on a ceramic-based chrono-typological sequence. The latter in particular has been
168 central to Japanese archaeology, and nearly a century of painstaking research has led to the
169 creation of detailed regional and sub-regional sequences. As a result, archaeologists utilise
170 more often such relative sequences, rather than absolute calendar dates, when referring to
171 key episodes and events within the Jōmon period.

172
173 Given its time span of over 10,000 years, it is perhaps unsurprising that the Jōmon period was
174 characterised by multiple episodes of population booms and busts, typically inferred from
175 fluctuations in the number of residential units (pit-dwellings) and archaeological sites. Early
176 works (Koyama 1978) have initially identified major regional trends (a slow rise in the
177 Southwest, a rise and fall in the centre, and rise followed by a plateau in the North) at a
178 millennial-scale. However, subsequent studies based on chrono-typological sequences (e.g.
179 Imamura 1997, Shitara 2004, Sekine 2014, etc.) have revealed a much more complex picture,
180 with multiple fluctuations and further regional and sub-regional variation in the demographic
181 trajectories. These studies provide a much-refined perspective on Jōmon demography,
182 potentially capturing key processes such as population dispersal and differences in local
183 adaptive strategies to environmental change. However, the over-reliance on ceramic-based
184 chronology severely limits the possibility to explore these hypotheses by, for example,
185 comparing these dynamics to climatic data, or to infer key measures such as population
186 growth rate accurately. The *dates as data* provide one way to overcome these issues (see
187 Crema et al 2016 for an application on Jōmon data) but should ideally be coupled with
188 alternative proxies to evaluate its robustness as a measure of past demographic change.

189
190 Assigning absolute calendar dates to the Jōmon chrono-typological sequence is thus an
191 important step for further exploring its population dynamics, and at the same bring in additional
192 lines of evidence to test specific hypothesis linked to social, economic, and cultural factors.
193 This objective becomes even more appealing if we consider that the total number of chrono-
194 typological phases and subphases across the entire length of the Jōmon period is easily above
195 100 (cf. Kobayashi, T. 2008). This fine-grained scheme had led some scholars to suggest that
196 the duration of several phases might be less than 100 years (e.g. Kobayashi, K 2008), an
197 unmatched resolution for prehistoric hunter-gatherers. However, attempts to construct an
198 absolute chronological framework for these ceramic phases have been comparatively limited.
199 Most studies have focused on the visual display of calibrated radiocarbon dates associated
200 with key ceramic phases, which has already revealed putative relationships between major
201 cultural and climatic events throughout the Jōmon period (e.g. Kudo 2007).

202
203 More recently, Kobayashi (2008, 2017) has collated and analysed a sample of over 3,200
204 radiocarbon dates to develop an absolute chronology of the start and end dates of major
205 Jōmon ceramic phases. Kobayashi's chrono-typological sequence has subsequently been
206 used to construct time-series of residential units counts for different regions (Kobayashi, K.
207 2008, Crema 2012, Crema 2013), confirming the existence and assessing the timing of at
208 least three cycles of population rise and fall between the Early and the Late Jōmon periods
209 (ca 7000- 3200 cal BP) in central Japan.

210
211 However, Kobayashi's sequence assumes perfectly abutting phases (i.e. the start of a ceramic
212 phase coincides to the end of the previous phase), no uncertainty in the dates, and an agnostic
213 view on the *within-phase uncertainty*. As a consequence, some analyses showed a false
214 impression of high accuracy and precision when abrupt changes in the number of residential

215 units were recorded between chronologically adjacent phases. To overcome this issue, here
216 we model Jōmon ceramic phases allowing for overlaps and model the *within-phase*
217 *uncertainty* using the trapezoidal distribution. The latter allows to take into the assumption of
218 a rise and fall pattern in the popularity of cultural traits while allowing for the flexibility to take
219 different shapes (see Lee and Bronk-Ramsey 2012). We employ Bayesian inference to fully
220 take into account the uncertainty in the estimates of model parameters and use a nested form
221 of Monte-Carlo simulation to sample absolute calendar dates of archaeological events while
222 taking into account all three forms of uncertainty described above.

223
224 Our case study re-examines a dataset of Jōmon pit-dwellings from southwest Kanto (Saitama,
225 Tokyo, and Kanagawa prefectures) and Chubu Highlands (Nagano and Yamanashi
226 prefectures) in central Japan as a case study. The dataset has been originally studied by
227 Imamura (1997) and re-examined by Crema (2012). We then compare the time-series of
228 residential frequencies we obtained from the two regions to the summed probability distribution
229 (SPD) of radiocarbon dates from the same area, examining, in particular, the timing of the
230 Middle Jōmon rise-and-fall, the largest demographic fluctuation recorded in this area during
231 the Jōmon period. Given the smaller number sample size for earlier periods we focus on the
232 interval between 8,000 and 3,000 cal BP, corresponding approximately to the latter half of the
233 Initial Jōmon to the end of the Final Jōmon period.

234 **Materials**

235 We collated radiocarbon dates with known association to Jōmon ceramic phases by
236 augmenting an existing database created by one of us (see Kobayashi 2017). The initial
237 dataset has been cleaned by removing duplicates, samples with incomplete information, as
238 well as dates from specimens with suspected marine reservoir effect. The resulting, final
239 dataset consisted of 2,120 radiocarbon dates from 447 archaeological sites across Japan (see
240 electronic supplementary table 1). We used a revised form of Kobayashi's ceramic phases
241 (**Table 1**; see also Kobayashi 2017) by aggregating shorter and small-sampled sub-phases
242 together. The resulting sequence comprised 42 ceramic phases covering the entire
243 chronological span of the six major Jōmon periods (Initial, Incipient, Early, Middle, Late, and
244 Final Jōmon). Samples of soot and organic residues taken from the same vessel were
245 combined using OxCal's *R_Combine* function under the assumption that the dates were
246 associated with the same calendar year.

247
248 The residential data used by Imamura's (1997) and Crema's (2012) study was collated by
249 digitising summary tables from Suzuki (2006). This consisted of dwelling counts organised by
250 ceramic phases with different degrees of uncertainty ranging from associations to a single
251 phase to as many as 14 phases (see Crema 2012 for an extensive discussion). The 9,612
252 Jōmon pit-dwellings in the dataset were collated from Yamanashi (n= 501), Tokyo (n=2,221),
253 Saitama (n=1,748), Kanagawa (n=2,724), and Nagano (n=2,418) prefectures in central Japan.
254 The sample includes few pit-dwellings dated to the Incipient, Initial, and Final Jōmon periods
255 which are outside the temporal window of analyses in the majority of the Monte-Carlo samples
256 of ceramic phase start and end dates. Nonetheless, we decided to keep the entire dataset, as
257 this has no impact in the approach we employed other than the frequency time-series being
258 composed of slightly different sample sizes for each Monte-Carlo iteration.

259
260 For the SPD analysis, we collated a total of 2,544 radiocarbon dates from 370 sites located in

261 the same regions have been retrieved from the National Museum of Japanese History's
262 radiocarbon database (Kudo 2017, URL: <https://www.rekihaku.ac.jp/up->
263 [cgi/login.pl?p=param/esrd/db_param](https://www.rekihaku.ac.jp/up-cgi/login.pl?p=param/esrd/db_param), electronic supplementary table 2). The initial data
264 obtained from the online query included all dates associated with terrestrial and marine
265 samples attributed to the Jōmon period from the five prefectures. We excluded, from this initial
266 set, duplicates, dates from bones with unknown impact of reservoir effect ($n=13$), as well as
267 samples with a ^{14}C age outside the bracket 7,500 ~ 2,500 ^{14}C Age (ca. 8000 ~ 3000 cal BP).
268 The final dataset consisted of 1,550 radiocarbon dates from 283 sites, with 77 dates also
269 included in the samples used for the Bayesian chronological modelling.

270 [TABLE 1 HERE]

271 **Table 1** Correspondence between different nomenclature of ceramic phases and associated
272 sample size of radiocarbon dates (n = number of radiocarbon dates, $n(\text{eff.})$ = number of
273 radiocarbon dates associated to different specimens; and *Sites* = number of archaeological
274 sites from which samples were recovered). * *Kasori E* ceramic phases have two distinct
275 classifications using Arabic and Roman numerals (see detailed review in Toda 1999).

276

277 **Methods**

278 *Bayesian Chronological Modelling*

279 We fitted trapezoidal models (Lee and Bronk Ramsey 2012) to the 42 Jōmon ceramic phases
280 using *OxCal* v.4.3 (Bronk Ramsey 2009a) and bespoke R scripts to handle input/output via
281 the *oxcAAR* v1.0 R package (Hinz et al. 2018). The choice of the trapezoidal model over other
282 distributions was dictated by its flexibility in capturing a variety of possible shapes to portray
283 within-phase uncertainty, including uniform distribution and single-peaked symmetric
284 distributions comparable to the Gaussian. In order to evaluate the sensitivity of our outcome
285 to the choice of this model we also fitted Gaussian and Uniform models which produced results
286 that were qualitatively comparable to the ones presented in the paper (see electronic
287 supplementary figures 1-4).

288

289

290 Radiocarbon dates associated with the same event (e.g. the same ceramic vessel) were
291 combined using the *R_Combine* function in *OxCal* after removing potential outliers (Bronk
292 Ramsey 2009b) using a normal distribution model with a mean of zero and a standard
293 deviation of 2. This was achieved by removing the date with the highest outlier probability and
294 by repeating the process iteratively until the overall agreement index was above 60 and the
295 Chi-squared test was non-significant at $\alpha=0.05$.

296

297 The initial fitting of the trapezoidal model for the 42 ceramic phases returned an overall
298 agreement index of 48. We thus removed a total of 46 dates with agreement indices below 60
299 and refitted our model achieving an overall agreement index of 110.86. We then used the

300 *MCMC_Sample* function in OxCal and extracted 5,000 posterior samples of the four
301 trapezoidal distribution parameters for each of the 42 ceramic phases.

302 *Monte-Carlo Simulation*

303 We simulated calendar dates for each pit-dwelling in three steps:

304

- 305 1. Sample the four parameters of the trapezoidal model from the joint posterior
306 distribution of each of the 42 ceramic phases.
- 307 2. Randomly assign a unique phase to all pit-dwellings associated with multiple
308 candidate phases. The probability of a candidate phase being selected was
309 proportional to its standard deviation, calculated using the equation provided by Dorp
310 and Kotz (2003) for trapezoid distributions. For example, if a residential unit was
311 assigned to phases *I*, *II*, and *III*, with standard deviations 20, 30, and 50, the
312 probability of the assigned phase being *I* is equal to 0.2 (i.e. $20/(20+30+50)$).
- 313 3. Randomly draw a calendar date from the trapezoidal distributions defined in step 1
314 and associated with a given residential unit in step 2.

315

316 This routine — which effectively takes into account within-phase, phase assignment, and
317 phase boundary uncertainties — was repeated 5,000 times. For each repetition set we also:
318 a) computed a univariate kernel density estimate of the simulated dates; and b) grouped and
319 counted residential units falling within 100-years sized temporal blocks between 8,000 and
320 3,000 cal BP (i.e. 8,000-7,901 cal BP; 7,900 - 7,801 cal BP; etc.).

321 *Summed Probability Distribution of Radiocarbon Dates*

322 A Summed Probability Distribution of Radiocarbon Dates (SPD) was created using the *rcarbon*
323 v.1.3 package (Bevan and Crema 2019). We calibrated the ^{14}C dates using the *IntCal13*
324 calibration curve (Reimer et al. 2013) and without normalisation to avoid artificial peaks (cf.
325 Weninger et al. 2015). Marine dates were calibrated with the *Marine13* calibration curve
326 (Reimer et al. 2013), using a ΔR of 88 and an associated error of 33 years (Shishikura et al.
327 2007). To account for inter-site variation in sampling intensity, we summed to unity dates from
328 the same site with a median calibrated age inter-distance of 200 years (cf. Timpson et al 2014,
329 see electronic supplementary figure 5 for sensitivity analysis with different inter-distance
330 settings). The resulting 768 “bins” have been combined to produce the final SPD curve. To
331 facilitate the comparison between different proxies we aggregated the summed probabilities
332 using the same 100-years temporal blocks between 8,000 and 3,000 cal BP used for the pit-
333 dwelling data. We also sampled random calendar dates from each of the 768 bins and
334 generated time-series of bin counts aggregated using the same 100-years temporal blocks.
335 This process was repeated 5,000 times in order to produce the same number of frequency
336 time-series as the residential units.

337 *Correlation Analysis and Model Testing*

338 We assessed the correlation between the two demographic proxies by computing 5,000
339 Pearson’s correlation coefficients between randomly paired 100-years block time-series of
340 radiocarbon bins and pit-dwelling counts. To explore possible temporal variations in the extent
341 of correlation between the two proxies we also calculated their rolling correlation using a
342 moving window of 10 time-blocks, equivalent to a 1,000 years.

343

344 In order to further explore differences between the two demographic proxies, while taking into
345 account the idiosyncrasies of the calibration process and the effects of sampling error, we also
346 employed a modified version of the Monte Carlo testing approach used in Shennan et al.
347 (2013, see also Timpson et al. 2014). The original approach consists of 1) fitting a theoretical
348 growth model to the observed data; 2) simulating the same number of dates as the observed
349 data in calendar time using the fitted model; 3) back-calibrating each date in ^{14}C age and
350 calibrating it back in calendar time; 4) generating a realisation of the theoretical SPD by
351 summing the dates; and 5) repeating steps 1 to 4 multiple times to generate a simulation
352 envelope to which the observed SPD can be compared to. We made two notable changes to
353 this procedure. First, we generated our simulation envelope (representing our theoretical
354 expectation) from the mean value in the composite kernel density estimate of the residential
355 data rather than a fitted exponential curve. Thus, our null hypothesis was that changes in the
356 density of radiocarbon dates are comparable to changes in the density of residential units.
357 Second, we compared observed and simulated annual growth rates rather than the raw SPDs
358 to avoid the impact of early divergences in defining later differences between the two proxies.

359 Results

360 **Figure 1** shows the posterior distribution of the trapezoidal model parameters of the forty-two
361 Jōmon ceramic phases we examined. Although the Bayesian model did not include any
362 constraints on the temporal relationship between phases, our results confirmed the general
363 sequence expected from the literature, particularly when the “core stage” of each phase (i.e.
364 the interval between the parameters b and c) was considered. In very few cases the early tail
365 of the distribution (i.e. parameter a) exhibited reverse chronological order (e.g. $S2.1_a$ is
366 estimated to be more recent than $S2.2_a$; $S6_a$ is more recent than $S7_a$), but these exceptions
367 were limited to chrono-typological phases of the Initial Jōmon period where the number of
368 diagnostic elements in the ceramics are limited.

369

370 The increase in the number of more complex decorative elements does undoubtedly play a
371 significant role in explaining the more detailed periodisation and consequently the shorter
372 duration of ceramic phases in some temporal windows, most notably within the Middle Jōmon
373 period. These shorter phases (some possibly with sub-century durations) often have a higher
374 degree of overlap in their interval. In the case of the Middle Jōmon period, this pattern can at
375 least in part be explained by the presence of plateaus in the calibration curve (particularly
376 around 5,300 to 5,000 cal BP). More in general, and aside from the genuine existence of
377 overlaps between phases, it is worth considering that the model does not take into account
378 the spatial dimension, and consequently the diffusion of particular ceramic styles and the
379 resulting temporal discrepancy across sites located in different regions. These are, however,
380 acceptable limitations as the pit-dwelling data we examined are from central Japan which has
381 the most substantial contribution to the data we used to define our chronological model.
382 Nonetheless, targeted studies on smaller regions and/or explicit incorporation of the spatial
383 dimension are desirable if more accurate regional comparisons are being sought.

384

385

[FIGURE 1 HERE]

386

Figure 1. Marginal posterior distribution of the trapezoidal model parameters for the 42 Jōmon

387 ceramic phases.

388 [FIGURE 2 HERE]

389

390 **Figure 2** Composite kernel density estimates derived from the simulated dates of Jōmon pithouses
391 from Southwest Kanto (a) and Chubb highland (b). The envelope represents the 95% percentile interval
392 of the kernel densities across the 5,000 simulations, and the solid line the average value for each
393 calendar date.

394

395 **Figure 2** shows the composite plots of the kernel density estimates (CKDE; Brown 2017)
396 obtained from each of the 5,000 simulated sets of pit-dwelling dates from Southwest Kanto
397 (Kanagawa, Saitama, and Tokyo prefectures; **figure 2-a**) and Chubu highlands (Yamanashi
398 and Nagano prefectures; **figure 2-b**). Both sets of curves capture the main demographic
399 fluctuations depicted in Imamura's original study (cf. fig.2 in Imamura 1997), including the
400 Early Jōmon rise and fall (ca. 6,500~5,800 cal BP) and the minor oscillations between the end
401 of Middle Jōmon and the first half of the Late Jōmon period (ca. 4,600-4,000 cal BP) observed
402 in Southwest Kanto, and most notably the Middle Jōmon boom and bust (ca. 5,500-4,600 cal
403 BP) observed in both regions.

404 [FIGURE 3 HERE]

405

406 **Figure 3.** Temporal frequencies of residential units (a) and summed probability of radiocarbon dates
407 (b) and their correlation over a 1,000 years moving window (c). Error bars in panel a and the grey
408 envelope in panel c are based on 95% percentile interval across the 5,000 Monte Carlo simulations.

409

410 The combined time-series of the two regions (**figure 3-a**) shows broad similarities in shape
411 with the SPD generated from the radiocarbon dates of the five prefectures (**figure 3-b**). The
412 latter also exhibits boom and bust events over the same interval, although with some
413 discrepancies in their timing (see below), the lack of a rise-and-fall pattern in the mid 5th
414 millennium cal BP, and a comparatively higher density of dates from 4,700 cal BP onwards.
415 Despite these differences, the overall sample correlation between the two time-series across
416 the 5,000 Monte-Carlo iterations was high (median: $r = 0.65$; 95% percentile interval: 0.51 -
417 0.75) and the 1,000 years rolling correlation (**figure 3-b**) suggest a generally high agreement
418 between the time-series of radiocarbon dates and pit-dwellings.

419

420 The discrepancies in the timing of the Middle Jōmon rise and fall between the 6th and the 5th
421 millennium cal BP are further highlighted in **figure 4**, where the observed annual growth rate
422 computed from the radiocarbon dates is compared against a theoretical envelope of growth
423 rates simulated from the observed residential data. The analysis confirms intervals when the
424 SPD-based growth rates diverge significantly from the expectation derived from residential
425 data, with lower rates around 5,500-5,350 and 5,100-4,900 cal BP, and higher rates around
426 4,800-4,300 and 4,000 cal BP.

427

428 [FIGURE 4 HERE]

429

430 **Figure 4.** Statistical comparison of the observed annual growth rate in the SPD (solid line) and the
431 simulated 95% percentile envelope based on the temporal frequencies of residential units obtained

432 *from composite kernel density estimate analysis. Regions highlighted in red indicate intervals where*
433 *the SPD-based growth rate is higher than the growth rates based on pit-dwelling density. Regions*
434 *highlighted in blue suggest the opposite (i.e. lower growth rates in the SPD). The temporal range of*
435 *the analyses is reduced by 400 years on both ends to limit edge effects. The global P-value was*
436 *equal to 0.0009.*

437 **Discussion**

438 The Bayesian chronological model presented here is most likely the first of many attempts in
439 providing a more accurate chrono-typological sequence for the Jōmon period. We intentionally
440 decided to not present point-estimates of the start/end date of the ceramic phases to avoid
441 conveying a false impression of a precision that cannot be realistically achieved. We argue,
442 instead, that conversions from a relative to an absolute chronological framework should fully
443 embrace all forms of uncertainty, including those defining the chronological boundaries of
444 individual phases and periods.

445
446 Our case study demonstrates the importance and implications of defining a statistical
447 framework for chrono-typological phases. This paper constitutes the third attempt, after
448 Imamura (1997) and Crema (2012), in generating a time-series of pit-dwelling frequency
449 based on the same original data. Although both previous works and our analyses have
450 highlighted comparable fluctuations in the number of residential units, there are some notable
451 differences in the timing of these events that are worth noting. Perhaps the most relevant case
452 is the Middle Jōmon rise and fall. Imamura's (1997) original work was based on an earlier
453 chronology based on uncalibrated dates, with the rise of the Middle Jōmon "boom" dated at
454 ca. 5,000 bp (ca. 5700 cal BP) and the decline after 4,400 bp (ca 5000 cal BP), while Crema's
455 (2012) reassessment suggested the rise starting from 5,500 cal BP and the decline from 4,700
456 cal BP. Our analysis has instead revealed that the increase in population size started at 5500
457 cal BP (confirming the results of Crema 2012) with the decline stage starting as earlier as
458 4,900 cal BP (thus somewhat closer to Imamura's original estimate). The implication of an
459 earlier onset of the Middle Jōmon decline is particularly noteworthy as it cast further doubts
460 on the established narrative of a mid-5th millennium cooling or the 4.2k event as a driver of
461 the population decline (c.f. Imamura 1997, Yasuda 2004, Suzuki 2009, Tsuji 2013, Taniguchi
462 2019).

463
464 The absolute chronological framework offered by the combination of Bayesian modelling and
465 Monte-Carlo simulation has also enabled an evaluation of the *dates as data* approach,
466 following similar works carried out by few others (e.g. Palmisano et al. 2017, Tallavara and
467 Pesonen 2018). Our results indicate an overall agreement across the two proxies, reinforcing
468 the evidence of multiple episodes of possible demographic fluctuations between 8,000 and
469 3,000 years ago. However, we also identified several notable discrepancies: the SPD curve
470 shows an earlier timing of the Middle Jōmon rise-and-fall and an overall higher relative density
471 of dates during the Late and Final Jōmon (i.e. ca 4,500 to 3,000 cal BP).

472
473 One plausible explanation for these discrepancies is the major shift from nucleated to a
474 dispersed settlement pattern between the Middle and the Late Jōmon periods (Taniguchi
475 2005, Crema 2013, see Palmisano et al. 2017 for similar interpretations in Central Italy). The
476 binning protocol used in this paper and elsewhere (cf. Timpson et al. 2014) reduces the effect
477 of inter-site variation in sampling intensity, but effectively makes the SPD a proxy of settlement

478 density that disregards size variation. It follows that if the number of settlements is reduced,
479 but the average size increased due to nucleation, the SPD might signal a decline while the
480 time series of residential density show the opposite trend. Similarly, an episode of dispersion
481 and settlement fission to smaller communities might show an increase in the SPD (larger
482 number of sites) matched with a decrease in residential density (smaller number of residential
483 units).

484
485 Thus one possible hypothesis that could explain the mismatch observed in **figure 3** can be
486 summarised as follows: 1) the faster (and earlier) increase in the SPD around 5400 cal BP is
487 the result of an episode of territorial expansion and repeated episodes of settlement fission;
488 2) the subsequent decline in the SPD during the peak in residential density is the outcome of
489 settlement nucleation and population growth; and 3) the overall higher relative density of SPD
490 during the first few centuries of the 5th millennium is a signature of fission events to smaller
491 settlements. A similar small mismatch between site counts and dwelling counts have been
492 observed elsewhere and has indeed been explained by episodes of nucleation/dispersions
493 (e.g. Crema 2013, see also below). Unfortunately, the pit-dwelling count data provided by
494 Suzuki does not record membership of individual pit-dwelling to specific settlements, and
495 hence this hypothesis cannot be directly tested in this context by comparing the SPD to a time-
496 series of occupied settlements.

497
498 Archaeological evidence does, however, suggest several significant changes in the settlement
499 pattern during the second half of the Middle Jōmon period (phases C11~C14 here).
500 Stratigraphic evidence shows an overall decrease in the occupational span of individual pit-
501 dwellings between the Kasori E2 (phase C11) and the Kasori E3 (phase C12) phases, with
502 the latter characterised by shorter, repeated re-occupations in large nucleated settlements
503 (Kobayashi 2016). As a consequence, the same temporal window was characterised by a
504 higher number of residential units that do not necessarily translate into an increase in the
505 underlying population size. During the subsequent Kasori E4 phase (phase C13) these large
506 settlements fissioned into smaller sites, with a much shorter occupational span that suggests
507 an increased level of residential mobility (Kobayashi 2004). This shift from nucleated to
508 dispersed settlement patterns have been commonly explained as the consequence of a
509 change in subsistence economy triggered by the 4.2 cooling event (c.f. Suzuki 2009).
510 However, the possibility of local resource overexploitation cannot be dismissed, especially
511 considering how the cooling event has most likely occurred after the shift in settlement pattern
512 and the decline in the number of pit-dwellings (Kobayashi 2004). An interesting parallel could
513 also be drawn to the growth and decline of major Jōmon settlements such as Sannai-
514 Maruyama in Northern Japan. Habu (2008) hypothesise that a plant-based subsistence
515 intensification (e.g. chestnuts and other nuts) sustained the initial growth of this and possibly
516 other settlements in the region. This increased over-specialisation, however, made Jōmon
517 communities overpopulated and increasingly less resilient to episodes of minor climatic
518 fluctuations affecting plant productivity, eventually leading to the demise of large nucleated
519 settlements. Similar 'rigidity traps' (Carpenter and Brock 2008) might have occurred in Central
520 Japan as well, but further studies integrating demographic, climatic, and subsistence data will
521 be necessary to explore this hypothesis in detail.

522
523 The availability of an absolute chronological framework enables us to make tentative estimates
524 of the annual percentage growth rate observed during the Jōmon period. For example, the
525 annual growth rate during the Middle Jōmon "boom" (between 5,500-5,400 and 5,000-4,900

526 cal BP) was 0.45% (95% percentile interval: 0.33~0.74%) for the pit-dwelling data and 0.09%
527 (95% percentile interval: -0.01~0.21%) for the radiocarbon dates, an order of magnitude
528 above the long-term average recorded for hunter-gathers elsewhere (see Zahid et al. 2016)
529 but within the range expected for shorter-term fluctuations (see also Bettinger et al. 2016).
530 The discrepancies between the two figures are in part due to the different timing of the events
531 (see figure 3), and the fact that the SPD should be interpreted as a proxy of settlement growth
532 rate rather than population growth rate.

533

534 While these are promising results, there are several challenges both from the standpoint of
535 paleo-demographic inference and the methods presented here. Aside from shifts in settlement
536 pattern, we also need to consider potential changes in the *duration* of archaeological events.
537 Both intra- and inter-annual variations in the length of site occupation could change the ratio
538 between site counts and population size and hence, for example, potentially lead to false
539 signals in SPD depending on the choice of the bin size for aggregating radiocarbon dates from
540 the same site. The same problem applies to the duration of residential units (see above).
541 Ethnographic accounts and archaeological evidence suggest that pit-dwellings can have
542 different duration, lasting somewhere between 3 to 15 years (Watanabe 1986, Muto 1995).
543 Variations in residential stability can thus yield higher or lower number pit-dwellings in a given
544 time-window. In the case of Jōmon period, Kobayashi (1991) has inferred from the number of
545 seasonal rebuildings of hearths a maximum use of 8 years for Initial Jōmon pit-dwellings, while
546 for the late Middle Jōmon period, stratigraphic evidence of overlapping features and ¹⁴C dates
547 suggest an average occupation span of ca. 13 years, suggesting temporal variations in the
548 use-life of residential units (Kobayashi 2004). Habu (2001) has also extensively examined
549 residential data and lithic assemblage of the second half of the Early Jōmon period in the same
550 area, providing evidence for sub-regional variations and temporary shifts between collector
551 and forager-like strategies.

552

553 The development of a reliable regional Bayesian chronological model of archaeological
554 phases has also its own challenges. While in stratigraphic contexts many of the assumptions
555 that act as priors and/or constraints in the chronological modelling can be well supported, the
556 same degree of confidence cannot be easily justified when we are considering multiple sites
557 located in a wider geographic area and examined potentially with different sampling strategies.
558 For example, a strongly imbalanced data might “pull” the posterior estimates of a particular
559 ceramic phase towards the occupation period of a particular site that happened to have a
560 larger sample of radiocarbon dates. The use of hierarchical models (cf. Banks et al. 2019), or
561 the formal integration of the spatial dimension are desirable directions to be undertaken in
562 order to solve at least some of these issues.

563 **Conclusion**

564 Notwithstanding the challenges entailed by developing Bayesian models of chrono-typological
565 sequences, the ability to use an absolute chronological framework while simultaneously
566 accounting for different forms of uncertainty is a crucial step for reusing legacy data in
567 archaeology. Our case study showcases both the necessity and the potential benefits of such
568 an endeavour, particularly in the context of prehistoric demography where the lack of
569 alternative proxies to radiocarbon dates can severely limit the assessment of the reliability of
570 demographic reconstructions as well as the opportunity to identify and test key covariates and
571 hypotheses.

572
573
574
575
576
577
578
579
580
581

From the perspective of Jōmon archaeology, the comparison between SPDs and residential data has provided an initial assessment of the temporal scale at which settlement dynamics can no longer be ignored, and the choice of the population proxy becomes relevant. At coarser temporal scales of 500~1000 years the agreement between the two proxies is robust and reassuring, but below these thresholds, we identified some noticeable differences in the timing and the magnitude of specific fluctuations that need to be accounted for. These conclusions are context-specific and while they cannot be easily extrapolated to other regions or periods, offer the foundation for future research in prehistoric demography.

582 **Acknowledgements**

583 This research was funded by the ERC grant Demography, Cultural Change, and the Diffusion
584 of Rice and Millets during the Jōmon-Yayoi transition in prehistoric Japan (ENCOUNTER)
585 (Project N. 801953, PI: Enrico Crema). We would like to thank the two reviewers (David Orton
586 and an anonymous) for their constructive comments that helped improve the original
587 manuscript.
588
589

590 **Figure Captions**

591 **Figure 1.** Marginal posterior distribution of the trapezoidal model parameters for the 42 Jōmon
592 ceramic phases.

593
594 **Figure 2** Composite kernel density estimates derived from the simulated dates of Jōmon pit-dwellings
595 from Southwest Kanto (**a**) and Chubb highland (**b**). The envelope represents the 95% percentile interval
596 of the kernel densities across the 5,000 simulations, and the solid line the average value for each
597 calendar date.

598
599 **Figure 3.** Temporal frequencies of residential units (**a**) and summed probability of radiocarbon dates
600 (**b**) and their correlation over a 1,000 years moving window (**c**). Error bars in panel **a** and the grey
601 envelope in panel **c** are based on 95% percentile interval across the 5,000 Monte Carlo simulations.
602

603
604 **Figure 4.** Statistical comparison of the observed annual growth rate in the SPD (solid line) and the
605 simulated 95% percentile envelope based on the temporal frequencies of residential units obtained
606 from composite kernel density estimate analysis. Regions highlighted in red indicate intervals where
607 the SPD-based growth rate is higher than the residential density based growth rates. Regions
608 highlighted in blue suggest the opposite (i.e. lower growth rates in the SPD). The temporal range of
609 the analysis is reduced by 400 years on both ends to limit edge effects. The global P-value was equal
610 to 0.0009.

611
612
613
614
615
616

617 **References**

618

619 Anzai, M. 2019. Chiiki shūdan no han-ei - Jōmon jidai, chū. Tokyo: Keibunsha. (In
620 Japanese).

621

622 Attenbrow, V., Hiscock, P., 2015. Dates and demography: are radiometric dates a robust
623 proxy for long-term prehistoric demographic change? *Archaeology in Oceania* 50, 30–36.
624 <https://doi.org/10.1002/arco.5052>

625

626 Banks, W.E., Bertran, P., Ducasse, S., Klaric, L., Lanos, P., Renard, C., Mesa, M., 2019. An
627 application of hierarchical Bayesian modeling to better constrain the chronologies of Upper
628 Paleolithic archaeological cultures in France between ca. 32,000–21,000 calibrated years
629 before present. *Quaternary Science Reviews* 220, 188–214.
630 <https://doi.org/10.1016/j.quascirev.2019.07.025>

631

632 Baxter, M.J., Cool, H.E.M., 2016. Reinventing the wheel? Modelling temporal uncertainty
633 with applications to brooch distributions in Roman Britain. *Journal of Archaeological Science*
634 66, 120–127. <https://doi.org/10.1016/j.jas.2015.12.007>

635

636 Bellanger, L., Husi, P., 2012. Statistical tool for dating and interpreting archaeological
637 contexts using pottery. *Journal of Archaeological Science* 39, 777–790.
638 <https://doi.org/10.1016/j.jas.2011.06.031>

639

640 Bettinger, R.L., 2016. Prehistoric hunter–gatherer population growth rates rival those of
641 agriculturalists. *PNAS* 113, 812–814. <https://doi.org/10.1073/pnas.1523806113>

642

643 Bevan, A., 2015. The data deluge. *Antiquity* 89, 1473–1484.
644 <https://doi.org/10.15184/aqy.2015.102>

645

646 Bevan, A., Conolly, J., Hennig, C., Johnston, A., Quercia, A., Spencer, L., Vroom, J., 2012.
647 Measuring Chronological Uncertainty in Intensive Survey Finds. *Archaeometry* 55, 318–328.

648

649 Bevan, A., Colledge, S., Fuller, D., Fyfe, R., Shennan, S., Stevens, C., 2017. Holocene
650 fluctuations in human population demonstrate repeated links to food production and climate.
651 *PNAS* 114, E10524–E10531. <https://doi.org/10.1073/pnas.1709190114>

652

653 Bevan, A., Crema, E.R. 2019. rcarbon v1.3.0: Methods for calibrating and analysing
654 radiocarbon dates, "URL: <https://CRAN.R-project.org/package=rcarbon>.

655

656 Bronk Ramsey, C., 2009a. Bayesian Analysis of Radiocarbon Dates. *Radiocarbon* 51, 337–
657 360. <https://doi.org/10.1017/S0033822200033865>

658

659 Bronk Ramsey, C. 2009b. Dealing with outliers and offsets in radiocarbon dating.
660 *Radiocarbon*, 51, 1023-1045.

661

662 Bronk Ramsey, C., 2017. Methods for Summarizing Radiocarbon Datasets. *Radiocarbon* 59,
663 1809–1833. <https://doi.org/10.1017/RDC.2017.108>

664
665 Brown, W.A., 2017. The past and future of growth rate estimation in demographic temporal
666 frequency analysis: Biodemographic interpretability and the ascendance of dynamic growth
667 models. *Journal of Archaeological Science* 80, 96–108.
668 <https://doi.org/10.1016/j.jas.2017.02.003>
669
670 Buck, C.E., Meson, B., 2015. On being a good Bayesian. *World Archaeology* 47, 567–584.
671 <https://doi.org/10.1080/00438243.2015.1053977>
672
673 Buck, C.E., Litton, C.D., Smith, A.F.M., 1992. Calibration of radiocarbon results pertaining to
674 related archaeological events. *Journal of Archaeological Science* 19, 497–512.
675 [https://doi.org/10.1016/0305-4403\(92\)90025-X](https://doi.org/10.1016/0305-4403(92)90025-X)
676
677 Carlson, D.L., 1983. Computer analysis of dated ceramics: estimating dates and
678 occupational ranges. *Southeastern Archaeology* 2, 8-20.
679
680 Carpenter, S, Brock, W. 2008. Adaptive Capacity and Traps. *Ecology and Society* 13, no. 2
681 <https://doi.org/10.5751/ES-02716-130240>.
682
683 Chaput, M.A., Gajewski, K., 2016. Radiocarbon dates as estimates of ancient human
684 population size. *Anthropocene, AAG hum-induce envir chg* 15, 3–12.
685 <https://doi.org/10.1016/j.ancene.2015.10.002>
686
687 Christenson, A.L., 1994. A Test of Mean Ceramic Dating Using Well-Dated Kayenta Anasazi
688 Sites. *Kiva* 59, 297–317.
689
690 Collins- Elliott, S.A., 2019. Quantifying artefacts over time: Interval estimation of a Poisson
691 distribution using the Jeffreys prior. *Archaeometry* 61, 1207–1222.
692 <https://doi.org/10.1111/arcm.12481>
693
694 Contreras, D.A., Meadows, J., 2014. Summed radiocarbon calibrations as a population
695 proxy: a critical evaluation using a realistic simulation approach. *Journal of Archaeological*
696 *Science* 52, 591–608. <https://doi.org/10.1016/j.jas.2014.05.030>
697
698 Crema, E.R., 2012. Modelling Temporal Uncertainty in Archaeological Analysis. *Journal of*
699 *Archaeological Method and Theory* 19, 440–461.
700
701 Crema, E.R., 2013. Cycles of change in Jōmon settlement: a case study from Eastern Tokyo
702 Bay. *Antiquity* 87, 1169–1181.
703
704 Crema, E.R., 2015. Time and Probabilistic Reasoning in Settlement Analysis, in: Barceló,
705 J.A., Bogdanovic, I. (Eds.), *Mathematics and Archaeology*. CRC Press, Boca Raton, pp.
706 314–334.
707
708 Crema, E.R., Bevan, A., Lake, M., 2010. A probabilistic framework for assessing spatio-
709 temporal point patterns in the archaeological record. *Journal of Archaeological Science* 37,
710 1118–1130.

711
712 Crema, E.R., Habu, J., Kobayashi, K., Madella, M., 2016. Summed Probability Distribution of
713 14 C Dates Suggests Regional Divergences in the Population Dynamics of the Jōmon
714 Period in Eastern Japan. PLOS ONE 11, e0154809.
715 <https://doi.org/10.1371/journal.pone.0154809>
716
717 Crema, E.R., Bevan, A., Shennan, S., 2017. Spatio-temporal approaches to archaeological
718 radiocarbon dates. Journal of Archaeological Science 87, 1–9.
719 <https://doi.org/10.1016/j.jas.2017.09.007>
720
721 Crombé, P., Robinson, E., 2014. 14C dates as demographic proxies in Neolithisation models
722 of northwestern Europe: a critical assessment using Belgium and northeast France as a
723 case-study. Journal of Archaeological Science 52, 558–566.
724 <https://doi.org/10.1016/j.jas.2014.02.001>
725
726 Dorp, J.R. van, Kotz, S., 2003. Generalized trapezoidal distributions. Metrika 58, 85–97.
727 <https://doi.org/10.1007/s001840200230>
728
729 Downey, S.S., Bocaege, E., Kerig, T., Edinborough, K., Shennan, S., 2014. The Neolithic
730 Demographic Transition in Europe: Correlation with Juvenility Index Supports Interpretation
731 of the Summed Calibrated Radiocarbon Date Probability Distribution (SCDPD) as a Valid
732 Demographic Proxy. PLoS ONE 9, e105730. <https://doi.org/10.1371/journal.pone.0105730>
733
734 Dunnell, R.C., 1970. Seriation method and its evaluation. American Antiquity 35, 305–319.
735
736 Feeser, I., Dörfler, W., Kneisel, J., Hinz, M., Dreibrodt, S., 2019. Human impact and
737 population dynamics in the Neolithic and Bronze Age: Multi-proxy evidence from north-
738 western Central Europe. The Holocene 29, 1596–1606.
739 <https://doi.org/10.1177/0959683619857223>
740
741 Freeman, J., Byers, D.A., Robinson, E., Kelly, R.L., 2018. Culture Process and the
742 Interpretation of Radiocarbon Data. Radiocarbon 60, 453–467.
743 <https://doi.org/10.1017/RDC.2017.124>
744
745 Habu, J., 2001. Subsistence-Settlement Systems and Intersite Variability in the Moroiso
746 Phase of the Early Jōmon Period of Japan. International Monographs in Prehistory, Ann
747 Arbor.
748
749 Habu, J., 2004. Ancient Jōmon of Japan. University of Cambridge Press, Cambridge.
750
751 Habu, J., 2008. Growth and decline in complex hunter-gatherer societies: a case study from
752 the Jōmon period Sannai Maruyama site, Japan. Antiquity 82, 571–584.
753
754 Habu, J. and K. Okamura. 2017. Japanese archaeology today: new developments, structural
755 undermining and prospects for disaster archaeology. In Habu, J., Olsen, W., L'ape, P.V.
756 (Eds.) Handbook of East and Southeast Asian Archaeology, pp.11-25. Springer, New York.
757
758 Hinz, M., Schmid, C., Knitter, D., Tietze, C. 2018. oxcAAR: Interface to 'OxCal' Radiocarbon

759 Calibration. R package version 1.0.0. <https://CRAN.R-project.org/package=oxcAAR>
760
761 Huggett, J., 2020. Is Big Digital Data Different? Towards a New Archaeological Paradigm.
762 Journal of Field Archaeology 45, S8–S17. <https://doi.org/10.1080/00934690.2020.1713281>
763
764 Imamura, K., 1997. Jōmon jidai no jūkyōatosū to jinkō no hendō, in: Fujimoto, T. (Eds.), Jū
765 no kōkogaku. Dōseisha, Tokyo, pp. 45–60. (In Japanese)
766
767 Imamura, K. 1999. Jōmon no jitsuzō wo motomete. Yoshikawakōbunkan, Tokyo. (In
768 Japanese)
769
770 Johnson, I., 2004. Aoristic Analysis: seeds of a new approach to mapping archaeological
771 distributions through time., in: Ausserer, K.F., rner, W.B., Gorianny, M., ckl, L.K.-V. (Eds.),
772 [Enter the Past] the E-Way into the Four Dimensions of Cultural Heritage: CAA2003. BAR
773 International Series 1227. Archaeopress, Oxford, pp. 448–452.
774
775 Kintigh, K.W., Altschul, J.H., Beaudry, M.C., Drennan, R.D., Kinzig, A.P., Kohler, T.A., Limp,
776 W.F., Maschner, H.D.G., Michener, W.K., Pauketat, T.R., Peregrine, P., Sabloff, J.A.,
777 Wilkinson, T.J., Wright, H.T., Zeder, M.A., 2014. Grand Challenges for Archaeology.
778 American Antiquity 79, 5–24. <https://doi.org/10.7183/0002-7316.79.1.5>
779
780 Kobayashi, K. 1991. Jōmonjidai-sōkikōyō no minami-Kantō ni okeru kyōjū katsudō.
781 Jōmonjidai 2, 81-118. (In Japanese).
782
783 Kobayashi, K. 2004. Jōmonshakai-kenkyū no shinshiten: tanso 14 nendaisokutei no riyō.
784 Tokyo, Rokuichishōbō. (In Japanese).
785
786 Kobayashi, K., 2008. Jōmonjidai no rekinendai, in: Kosugi, Y., Taniguchi, Y., Nishida, Y.,
787 Mizunoe, W., Yano, K. (Eds.), Rekishi No Monosashi: : Jōmonjidai kenkyū no hennetai kei.
788 Douseisha, Tokyo, pp. 257–269. (In Japanese).
789
790 Kobayashi, K. 2016. Shūraku no kanjōka-keisei to jikan. In Kobayashi, K (Eds.), Kōkogaku no
791 Chihei 1, Tokyo, Rokuichishōbō. pp.65-93. (In Japanese).
792
793 Kobayashi, K. 2017. Jōmonjidai no jitsunendai, Dōseisha, Tokyo. (In Japanese).
794
795 Kobayashi, T., Hudson, M., Yamagata, M., 1992. Regional Organization in the Jōmon
796 Period. Arctic Anthropology 29, 82–95.
797
798 Kobayashi, T., 2008. Jōmondoki no yōshiki to keishiki. In Kobayashi, T. (Eds.) Sōran
799 Jōmondoki, Tokyo, Amu Promotion, pp. 2-12, (In Japanese).
800
801 Koyama, S., 1978. Jōmon Subsistence and Population. Senri Ethnological Studies 2, 1–65.
802
803 Kudo, Y., 2007. The Temporal Correspondences between the Archaeological Chronology
804 and Environmental Changes from 11,500 to 2,800 cal BP on the Kanto Plain, Eastern Japan.
805 The Quaternary Research 46, 187–194.

806
807 Kudo, Y. 2017. Isekihakkutsuchōsa-hōkokusho hōshasei-tansonendai sokutei database no
808 sakusei no torikumi. Nihondaiyonkigakkai kōen yoshi shū, 47, 22. (In Japanese).
809
810 Lee, S., Bronk Ramsey, C., 2012. Development and Application of the Trapezoidal Model for
811 Archaeological Chronologies. Radiocarbon 54, 107–122.
812 https://doi.org/10.2458/azu_js_rc.54.12397
813
814 Lucarini, G., Wilkinson, T., Crema, E.R., Palombini, A., Bevan, A., Broodbank, C., 2020. The
815 MedAfriCarbon Radiocarbon Database and Web Application. Archaeological Dynamics in
816 Mediterranean Africa, ca. 9600–700 BC. Journal of Open Archaeology Data 8, 1.
817 <https://doi.org/10.5334/joad.60>
818
819 Lyman, R.L., Harpole, J.L., 2002. A. L. Kroeber and the Measurement of Time's Arrow and
820 Time's Cycle. Journal of Anthropological Research 58, 313–338.
821
822 Marwick, B., 2017. Computational Reproducibility in Archaeological Research: Basic
823 Principles and a Case Study of Their Implementation. J Archaeol Method Theory 24, 424–
824 450. <https://doi.org/10.1007/s10816-015-9272-9>
825
826 Manning K, Timpson A, Colledge S, Crema E, Edinborough K, Kerig T, Shennan S, 2014.
827 The chronology of culture: a comparative assessment of European Neolithic dating
828 approaches. Antiquity 88, 1065–1080.
829
830 Manning, K., Colledge, S., Crema, E., Shennan, S., Timpson, A., 2016. The Cultural
831 Evolution of Neolithic Europe. EUROEVOL Dataset 1: Sites, Phases and Radiocarbon Data.
832 Journal of Open Archaeology Data 5. <https://doi.org/10.5334/joad.40>
833
834 McNutt, C.H., 1973. On the Methodological Validity of Frequency Seriation. American
835 Antiquity 38, 45–60. <https://doi.org/10.2307/279310>
836
837 McLaughlin, T.R., 2018. On Applications of Space–Time Modelling with Open-Source 14C
838 Age Calibration. J Archaeol Method Theory. <https://doi.org/10.1007/s10816-018-9381-3>
839
840 Muto, Y., 1995. Minzokushi kara mita Jōmon-jidai no tateana-jūkyō. Teikyo Daigaku
841 Yamanashi bunkazai kenkyūjo kenkyū-hōkoku 6, 267–301. (In Japanese).
842
843 Neiman, F.D., 1995. Stylistic Variation in Evolutionary Perspective: Inferences from
844 Decorative Diversity and Interassemblage Distance in Illinois Woodland Ceramic
845 Assemblages. American Antiquity 60, 7–36.
846
847 O'Brien, M.J., Lyman, R.L. 2000. Applying Evolutionary Archaeology: A Systematic
848 Approach. New York: Kluwer Academic.
849
850 Oh, Y., Conte, M., Kang, S., Kim, J., Hwang, J., 2017. Population Fluctuation and the
851 Adoption of Food Production in Prehistoric Korea: Using Radiocarbon Dates as a Proxy for
852 Population Change. Radiocarbon 59, 1761–1770.
853

854 Ortman, S.G., 2014. Uniform Probability Density Analysis and Population History in the
855 Northern Rio Grande. *J Archaeol Method Theory* 1–32. [https://doi.org/10.1007/s10816-014-](https://doi.org/10.1007/s10816-014-9227-6)
856 [9227-6](https://doi.org/10.1007/s10816-014-9227-6)
857

858 Orton, D., Morris, J., Pipe, A., 2017. Catch Per Unit Research Effort: Sampling Intensity,
859 Chronological Uncertainty, and the Onset of Marine Fish Consumption in Historic London.
860 *Open Quaternary* 3. <https://doi.org/10.5334/oq.29>
861

862 Palmisano, A., Bevan, A., Shennan, S., 2017. Comparing archaeological proxies for long-
863 term population patterns: An example from central Italy. *Journal of Archaeological Science*
864 87, 59–72. <https://doi.org/10.1016/j.jas.2017.10.001>
865

866 Ratcliffe, J.H., McCullagh, M.J., 1998. Aoristic crime analysis. *International Journal of*
867 *Geographical Information Science* 12, 751–764.
868

869 Reimer, P.J., Bard, E., Bayliss, A., Beck, J.W., Blackwell, P.G., Ramsey, C.B., Buck, C.E.,
870 Cheng, H., Edwards, R.L., Friedrich, M., Grootes, P.M., Guilderson, T.P., Hafflidason, H.,
871 Hajdas, I., Hatté, C., Heaton, T.J., Hoffmann, D.L., Hogg, A.G., Hughen, K.A., Kaiser, K.F.,
872 Kromer, B., Manning, S.W., Niu, M., Reimer, R.W., Richards, D.A., Scott, E.M., Southon,
873 J.R., Staff, R.A., Turney, C.S.M., Plicht, J. van der, 2013. IntCal13 and Marine13
874 Radiocarbon Age Calibration Curves 0–50,000 Years cal BP. *Radiocarbon* 55, 1869–1887.
875 https://doi.org/10.2458/azu_js_rc.55.16947
876

877 Rick, J.W., 1987. Dates as Data: An Examination of the Peruvian Preceramic Radiocarbon
878 Record. *American Antiquity* 52, 55. <https://doi.org/10.2307/281060>
879

880 Riris, P., 2018. Dates as data revisited: A statistical examination of the Peruvian preceramic
881 radiocarbon record. *Journal of Archaeological Science* 97, 67–76.
882 <https://doi.org/10.1016/j.jas.2018.06.008>
883

884 Roberts Jr., J.M., Mills, B.J., Clark, J.J., Haas Jr., W.R., Huntley, D.L., Trowbridge, M.A.,
885 2012. A method for chronological apportioning of ceramic assemblages. *Journal of*
886 *Archaeological Science* 39, 1513–1520. <https://doi.org/10.1016/j.jas.2011.12.022>
887

888 Rogers, E. M. 1962. *Diffusion of innovations* (1st ed.). New York: Free Press of Glencoe.
889

890 Sekine T. 2014. Aomori-ken ni okeru Jōmon jidai no iseki-su no hensen. *The Quaternary*
891 *Research (Daiyonki kenkyū)* 2014; 53:193–203. (In Japanese.)
892

893 Shishikura, M., Echigo, T., Kaneda, H., 2007. Marine reservoir correction for the Pacific
894 coast of central Japan using ¹⁴C ages of marine mollusks uplifted during historical
895 earthquakes. *Quaternary Research* 67, 286–291.
896 <https://doi.org/10.1016/j.yqres.2006.09.003>
897

898 Shitara, H. 2004. Saiso no haikei - Jōmon/Yayoi jidai ni okeru kankyō hendō tonō taiōkankei.
899 *Kokuritsu rekishi minzoku hakubutsukan kenkyū hōkoku*, 112, 357-380 (In Japanese).
900

901 Shennan, S., Downey, S.S., Timpson, A., Edinborough, K., Colledge, S., Kerig, T., Manning,

902 K., Thomas, M.G., 2013. Regional population collapse followed initial agriculture booms in
903 mid-Holocene Europe. *Nature Communications* 4, ncomms3486.
904 <https://doi.org/10.1038/ncomms3486>
905
906 Shoda, S., 2007. A Comment on the Yayoi Period Dating Controversy. *Bulletin of the Society*
907 *of East Asian Archaeology* 1, 1–7.
908
909 Steponaitis, V.P., Kintigh, K.W., 1993. Estimating site occupation spans from dated artifact
910 types: some new approaches. In: Stoltman, J. (Ed.), *Archaeology of Eastern North America:*
911 *Papers in Honor of Stephen Williams*. Archaeological Report No. 25. Mississippi Department
912 of Archives and History, Jackson, pp. 349-361.
913
914 Surovell, T.A., Toohey, J.L., Myers, A.D., LaBelle, J.M., Ahern, J.C.M., Reisig, B., 2017. The
915 End of Archaeological Discovery, *American Antiquity* 1–13.
916 <https://doi.org/10.1017/aaq.2016.33>
917
918 Suzuki, Y., 2006. *Jōmonjidai shūraku no kenkyū*. Yūzankaku, Tokyo. (In Japanese).
919
920 Suzuki, Y. 2009. Kantō / Tōkai chihō no Jōmon shūraku to Jōmon shakai. In Suzuki, K.,
921 Suzuki, Y. (Eds.) *Shūraku no hensen to chiikisei*. Tokyo, Yūzankaku, pp 95-143. (In
922 Japanese).
923
924 Tallavaara, M., Pesonen, P., 2018. Human ecodynamics in the north-west coast of Finland
925 10,000–2000 years ago. *Quaternary International*.
926 <https://doi.org/10.1016/j.quaint.2018.06.032>
927
928 Taniguchi, Y. 2005. *Kanjōshūraku to Jōmon shakaikōzō*. Gakuseisha, Tokyo (In Japanese).
929
930 Taniguchi, Y. 2019. *Nyūmon Jōmonjidai no kōkogaku*. Dōseisha, Tokyo (In Japanese).
931
932 Timpson, A., Colledge, S., Crema, E., Edinborough, K., Kerig, T., Manning, K., Thomas,
933 M.G., Shennan, S., 2014. Reconstructing regional population fluctuations in the European
934 Neolithic using radiocarbon dates: a new case-study using an improved method. *Journal of*
935 *Archaeological Science* 52, 549–557. <https://doi.org/10.1016/j.jas.2014.08.011>
936
937 Toda, T., 1999 *Kantō-chihō chūki (Kasori E shiki)*. Jōmonjidai 10,298-307 (In Japanese).
938
939 Torfing, T., 2015. Neolithic population and summed probability distribution of 14C-dates.
940 *Journal of Archaeological Science* 63, 193–198. <https://doi.org/10.1016/j.jas.2015.06.004>
941
942 Tsuji, S. 2013. Jōmonjidai no nendai to rikuiki no seitaikeishi. In Izumi, T., Imamura, K.(Eds.)
943 *Kōza Nihon no kōkogaku 3: Jōmon-jidai 1*, pp. 61-81. (In Japanese).
944
945 Watanabe, H., 1986. Community Habitation and Food Gathering in Prehistoric Japan: An
946 Ethnographic Interpretation of the Archaeological Evidence, in: Pearson, R.J., Barnes, G.L.,
947 Hutterer, K.L. (Eds.), *Windows on the Japanese Past: Studies in Archaeology and*
948 *Prehistory*. Centre for Japanese Studies University of Michigan, Ann Arbor, pp. 229–254.
949

- 950 Williams, A.N., 2012. The use of summed radiocarbon probability distributions in
951 archaeology: a review of methods. *Journal of Archaeological Science* 39, 578–589.
952
- 953 Weninger, B., Clare, L., Jöris, O., Jung, R., Edinborough, K., 2015. Quantum theory of
954 radiocarbon calibration. *World Archaeology* 47, 543–566.
955 <https://doi.org/10.1080/00438243.2015.1064022>
956
- 957 Yasuda, Y. 2004, *Sekaishi no naka no Jōmon bunka* (3rd Ed.) Yūzankaku, Tokyo. (In
958 Japanese).
959
- 960 Zahid, H.J., Robinson, E., Kelly, R.L., 2016. Agriculture, population growth, and statistical
961 analysis of the radiocarbon record. *PNAS* 113, 931–935.
962 <https://doi.org/10.1073/pnas.1517650112>
963
- 964 Ziedler, J.A., Buck, C.E., Litton, C.D., 1998. Integration of Archaeological Phase Information
965 and Radiocarbon Results from the Jama River Valley, Ecuador: A Bayesian Approach. *Latin*
966 *American Antiquity* 9, 160–179.
967
968
969
970

Table

Period	Ceramic Phases	n	n (eff.)	Sites
End of Upper Palaeolithic	S0	16	16	4
Incipient Jomon	S1.1	64	62	16
	S1.2	77	77	24
	S2.1	94	90	20
	S2.2	38	38	8
Initial Jomon	S3	107	107	47
	S4	45	45	24
	S5	22	22	10
	S6	14	14	6
	S7	48	47	14
	S8	85	80	21
Early Jomon	Z1	56	50	16
	Z2	31	29	15
	Z3	55	53	8
	Z4	16	14	10
	Z5	59	55	15
	Z6	33	30	15
	Z7	29	29	16
Middle Jomon	C1	10	10	6
	C234	19	19	14
	C56	22	22	13
	C78	33	32	16
	C9	61	61	28
	C10	58	58	23
	C11	41	41	21

	C12	106	105	30
	C13	64	63	23
	C14	11	11	7
Late Jomon	K1	37	37	23
	K2	103	65	17
	K3	54	49	16
	K4	28	25	11
	K5	58	48	9
	K6	26	24	6
	K7	47	43	16
	K8	39	38	11
Final Jomon	B1	89	83	29
	B2	73	58	25
	B3	44	41	20
	B4	54	51	17
	B5	58	54	27
	B6	96	52	21

Kobayashi 2017	Ceramic Phase in Suzuki's Pithouse Data
S0	Mumon doki
S1-1	Ryūkisenmon-kei
S1-2	Biryūkisenmon-kei; Tsumegatamon-kei
S2-1	Tsumegatamon-kei; Ōnatsumon-kei
S2-2	Tajōmon-kei
S3-1	Igusa I; Igusa II; Daimaru; Natsushima; Inaridai; Tateno; Inarihara; Ōurayama; Hanawadai 1; Hanawadai 2; Hirasaka;
S3-2	
S3-3	
S3-4	
S4	Mito; Lower Tado; Upper Tado; Hosokubo
S5	Shiboguchi; Nojima
S6	Ugajimadai
S7	Lower Kayama; Upper Kayama
S8	Uenoyama; Irumi I; Irumi II ; Ishiyama; Okkōshi; Tenjinyama; Kaminokidai; Shioya; Shimoyoshii
Z1	Lower Hanazumi
Z2	Sekiyama; Futatsuki; Kaminoki
Z3	Kurohama; Ario
Z4	Moroiso a; Minamiōhara
Z5	Moroiso b; Uehara
Z6	Moroiso c; Hinata I; Kagobatake I; Shitajima
Z7	Jūsanbodai; Hinata II; Kagohata II
C1	Goryōgadai 1
C2~C4	Goryōgadai 2
C5	Atamadai 1a; Atamadai 1b; Mujinasawa;
C6	Katsuzaka I; Aramichi
C7	Atamadai 2; Atamadai 3; Katsuzaka 2; Tōnai I;
C8	Tōnai II;
C9a	Idojiri I; Idojiri III; Katsuzaka 3; Atamadai 4
C9bc	
C10a	Daigi 8a; Kasori E1 (EI)* Sori I
C10b	
C10c	
C11ab	Daigi 8b; Kasori E2 (EI)*; Sori II; Sori III
C11c	

C12a	
C12b	Daigi 9; Kasori E3 (EII-EIII)*; Sori IV;SoriV
C12c	
C13	Kasori E4 (EIV)*; Daigi 10;
-	Kasori EV; Daigi 10;
K1-1	
K1-2	Shōmyōji 1;Shōmyōji 2
K1-3	
K2	Horinouchi 1
K3	Horinouchi 2
K4	Kasori B1
K5	Kasori B2
K6	Kasori B3
K7	Takaihigashi; Sōya
K8	Angyō 1; Angyō 2
B1	Ōbora B; Angyō 3a
B2	Ōbora BC; Angyō 3b
B3	Ōbora C1; Angyō 3c; Maeura 1
B4	Ōbora C2; Angyō 3d; Maeura 2
B5	Ōbora A; Chiami; Kōri I
B6	Ōbora A'; Arami; Kōri II

Figure 1

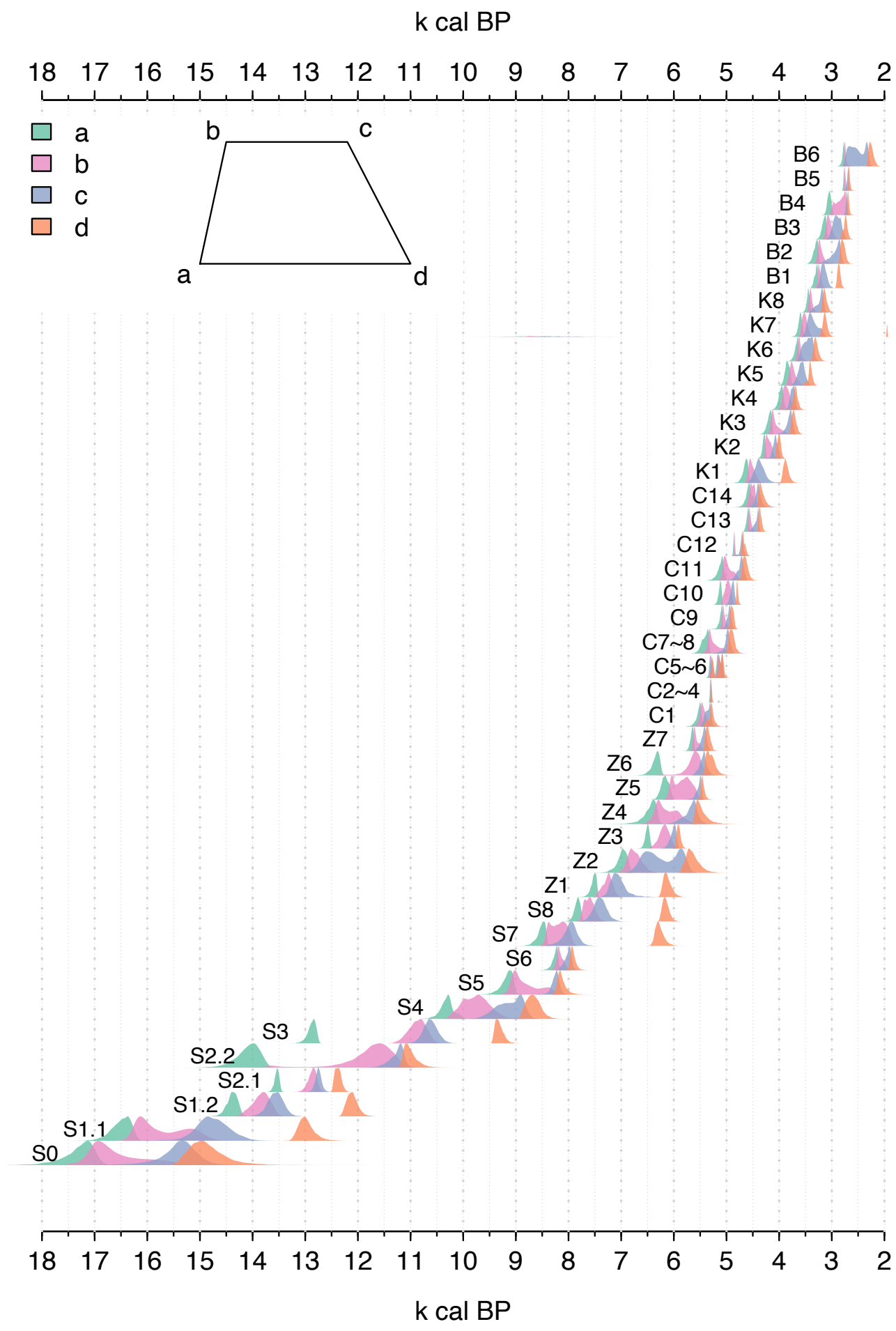


Figure 2

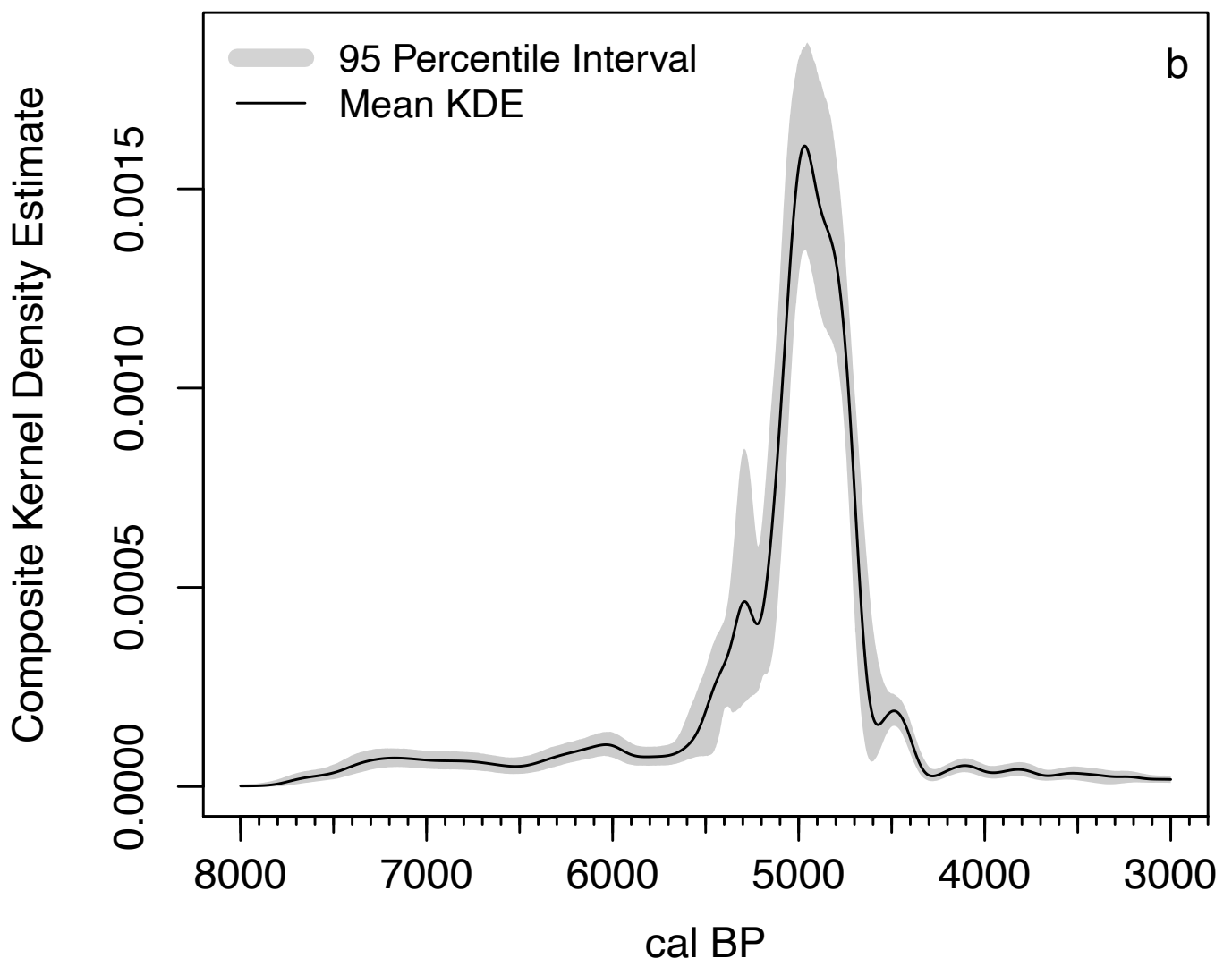
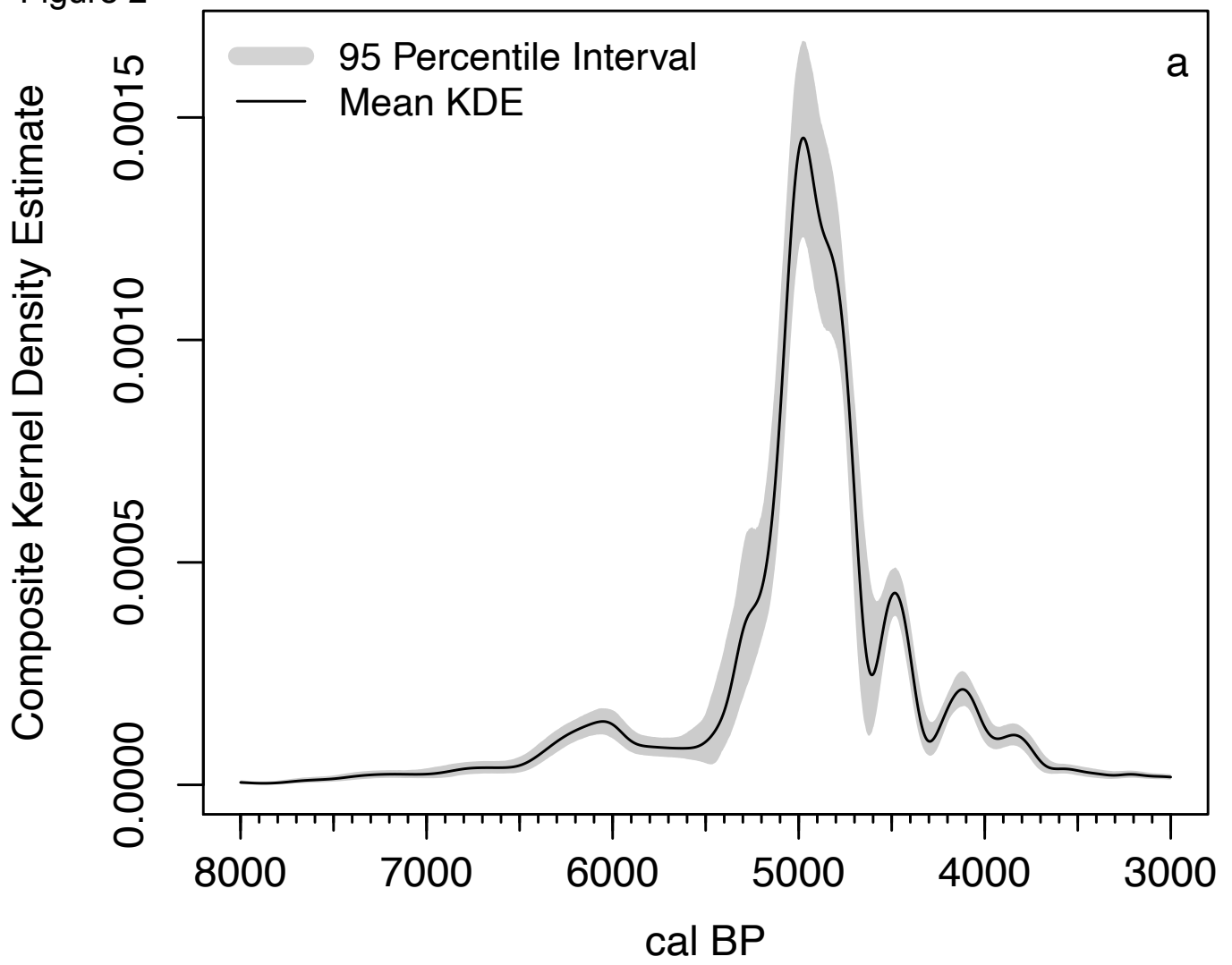


Figure 3

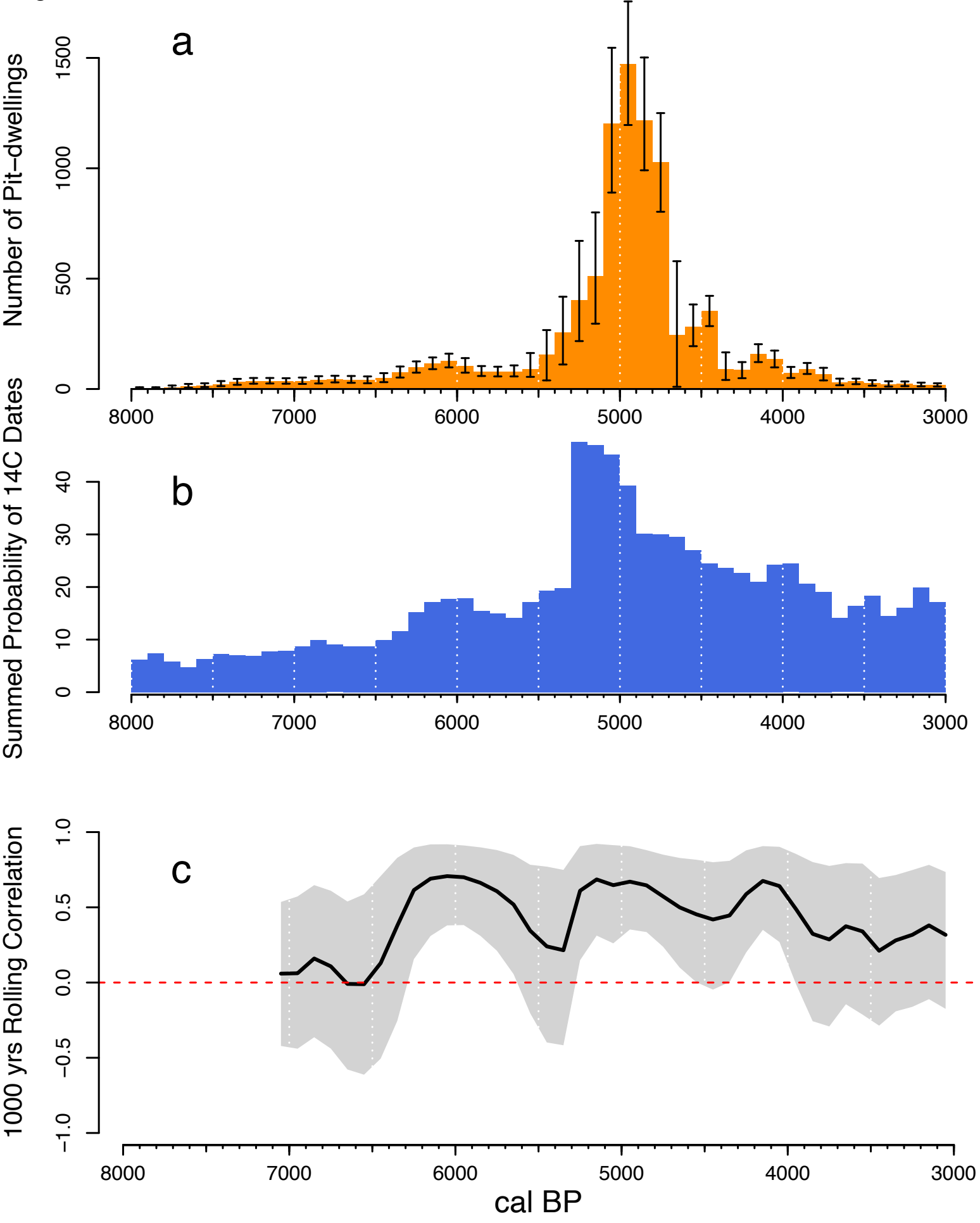


Figure 4

